Generating uniaxial vibration with an electrodynamic shaker and external air bearing

Daniel M. Harris and John W. M. Bush[1]

Department of Mathematics, Massachusetts Institute of Technology, 77 Massachusetts Ave., Cambridge, MA 02139

Abstract

Electrodynamic shakers are widely used in experimental investigations of vibrated fluids and granular materials. However, they are plagued by undesirable internal resonances that can significantly impact the quality of vibration. In this work, we measure the performance of a typical shaker and characterize the influence that a payload has on its performance. We present the details of an improved vibration system based on a concept developed by Goldman [1] which consists of a typical electrodynamic shaker with an external linear air bearing to more effectively constrain the vibration to a single axis. The principal components and design criteria for such a system are discussed. Measurements characterizing the performance of the system demonstrate considerable improvement over the unmodified test shaker. In particular, the maximum inhomogeneity of the vertical vibration amplitude is reduced from approximately 10% to 0.1%; moreover, transverse vibrations were effectively eliminated.

Keywords: Shaker design, Uniform vibration, Faraday waves

1. Introduction

The overall design of standard electrodynamic shakers is not dissimilar to that of a loudspeaker [2, 3]. Their primary feature is an armature assembly driven by a coil of wire subject to a radial magnetic field. The armature is

[1]Email address: bush@math.mit.edu

mechanically supported and positioned within the shaker housing by a flexure plate with low axial stiffness. A schematic of the cross-section of a typical electrodynamic shaker is shown in figure 1. While such traditional electrodynamic shakers are relatively robust and can generate a high level of force output, they often introduce undesirable transverse or rocking motions as a result of internal resonances [4]. This non-axial motion is of particular concern for calibrating accelerometers [5]. International standards for accelerometer calibration include guidelines as to the level of acceptable transverse motion [6]. Below 1000 Hz, transverse motion below 10% of the axial vibration amplitude is considered acceptable by these standards, however these limits are readily exceeded by typical flexure-based shakers [5].

One method to minimize transverse motion of the armature is by incorporating an air bearing slide in place of the flexures [7, 8]. This provides a high degree of lateral stiffness while maintaining nearly frictionless motion along axis. Several manufactures have begun to offer air-bearing shakers (e.g. The Modal Shop K394B30/B31), marketed primarily for accelerometer calibration applications. The payload capacity for such devices is generally quite low (less than 0.5 kg), severely limiting their range of utility for other applications. When both higher force capacity and uniaxial motion are required, other options must be pursued.

One option, the focus of this paper, is using a standard electrodynamic shaker with a flexure suspension and an external air bearing. Similar systems have been used in the past, primarily to study the behavior of vibrated granular media [1, 9, 10, 11, 12, 13, 14, 15, 16, 17] and also in studies of vibrated thin plates [18]. The frequencies of interest for these experiments generally range from 10 to 150 Hz. Non-axial vibration can be particularly detrimental to studies of vibrated granular materials, which can result in heaping [19, 20] as well as bulk rotation [1, 21]. The recent work of Aranson *et al.* [21] suggested that observations of large scale swirling motions of quasi-horizontal vibrated granular rods [22] may be due to unintended in-plane vibrations of the substrate. In particular, their experiments with an unmodified shaker and theoretical modeling suggest that the swirling motion is highly sensitive to the relative phase of the horizontal and vertical vibrations, which changes most rapidly near an internal resonant frequency of the shaker. They also noticed a significant shift in the shaker resonant frequency when switching from a monolayer of rice to steel rods, corresponding to an increase of only 0.18 kg in the mass of the payload. This is a striking example of an experiment where ignoring non-axial motions of the driver may lead to spurious conclusions.

Similar vibration systems incorporating an external air bearing have also been used to study Faraday waves [23, 24, 25, 26]. Above a critical value of the forcing amplitude known as the Faraday threshold, waves form spontaneously on the free surface [27, 28]. In studies of Faraday waves, spatial inhomogeneities of the forcing amplitude can lead to the formation of asymmetric surface wave patterns [29]. One option to attempt to compensate for nonuniform vibrational forcing amplitude is to dynamically balance the payload by positioning weights along the periphery of the fluid container until the Faraday waves appear to be uniformly excited at threshold [30]. However, an unbalanced payload could be potentially damaging to the shaker; furthermore, this process is time consuming and heuristic, and must be repeated with any change in the payload or driving. It is also unclear what impact this method has on the transverse motions of the shaker.

Our principal motivation for the development of a refined shaker system is for studies of oil droplets bouncing on the surface of a vibrated fluid bath below the Faraday threshold. These drops can walk spontaneously across the free surface through a resonant interaction with their own Faraday wave field [31, 32]. The walking drops exhibit many features of microscopic, quantum particles [33], including single-particle diffraction [34], tunneling [35], quantized orbits [36, 37, 38, 39], and wave-like statistics in confined geometries [40]. The analogue quantum behavior emerges just below the Faraday threshold where in the absence of the droplet, the surface remains flat. Typical studies of this system use vibration frequencies ranging from 20 to 150 Hz [41], but most commonly in the intermediate range of 50 to 80 Hz. Typical acceleration amplitudes are below $5g$, where g is the acceleration due to gravity. Driver payloads are typically on the order of a few kilograms. These hydrodynamic quantum analogue experiments define the parameter regime of interest in the present study. We have already successfully utilized the improved shaker system discussed in this work in our recent experimental investigations of the walking droplet system [42, 37].

Despite the numerous applications of electrodynamic shaker systems, details about their design and quantification of their performance benefits are extremely rare. Providing these details for our the system is the focus of the present work, which we hope will prove useful to those interested in the experimental modeling of hydrodynamic quantum analogues. In Section 2, we describe the details of the shaker as well as our measurement techniques. In Section 3, we present baseline measurements of our unmodified test shaker, which motivates the need for an improved design. In Section 4, we outline the details of the improved system and specify key design criteria. In Section 5, we present the test results of the improved system. Finally in Section 6, we summarize our conclusions and offer perspectives for future applications.

2. Experimental details

Throughout this work we use a Data Physics V55 electrodynamic shaker and PA300E amplifier as our driver, which is rated for a maximum sine force of 310 N and 12.7 mm peak-to-peak travel. It has a 76.2 mm diameter mounting table atop the armature with 9 threaded mounting holes. This shaker will be identified throughout as our “test shaker.” While the construction of our test shaker is typical of most standard shakers with flexure-plate suspensions, the precise characteristics and internal resonances will of course vary between manufacturers and models. Regrettably, data on transverse motion and spatial homogeneity of vibration is not readily available when purchasing a shaker. One specification that is commonly provided in the manufacturer’s literature is the armature resonance frequency, which refers to the frequency at which flexural resonances of the metal armature are excited. For our test shaker this frequency is listed as 7000 Hz ±5%, well above the typical operational frequencies for studies of granular media, Faraday waves, and bouncing droplets (< 150 Hz). One might thus naturally but mistakenly assume that such a shaker would provide high-quality driving for our experiments.

The shaker housing (43 kg) is bolted directly to a massive steel platform (54 kg) which can be leveled. An additional mass of 110 kg of granite blocks is added to the platform to further attenuate the vibration of the support structure. The leveling legs rest on rubber vibration-damping pads which reduce transmission of vibration to the floor.

In this study we measure accelerations using two miniature piezoelectric accelerometers (PCB, 352C65) weighing 2.0 grams each and with sensitivities of approximately 100 mV/g, where g is the acceleration due to gravity. For measurements of the homogeneity of vertical vibration, we stud mount the two accelerometers on diametrically opposed positions atop a precision ground aluminum plate, as shown in figure 2a. The hole for the stud is drilled and tapped normal to the mounting surface with an error of less than 1°. The mounting surface is cleaned before each installation and coated with a thin film of oil which fills any small voids in the surface, improving the vibration transmission to the sensor. The nominal calibration uncertainty for the sensors is ±1.5% for frequencies in the range of 10-99 Hz and ±1.0% for the frequencies in the range of 100-1999 Hz. The influence of these uncertainties on our assessment of vertical vibration homogeneity can be mitigated via a cross check of the accelerometer measurements. Specifically, we repeat each measurement twice, swapping the positions of the accelerometers on the second trial, and averaging the results. This mitigates any differences introduced exclusively by different calibration errors of the two accelerometers. Some measurement error naturally persists, which we refer to as "random error." Random error can be caused by environmental factors, transverse sensitivities of the accelerometers, and even differences in accelerometer cable routing and mounting torque [6]. We minimize measurement errors introduced by the accelerometer cable by routing the cable so that it does not contact the payload during operation. We also adjust the stationary cable routing point in order to avoid any transverse standing waves that can arise along the cable length. Furthermore, the shaker typically warms over hours of use [14], and the mechanical properties of its suspension may subsequently drift, leading to minor differences in performance between experiments. To assess the relative influence of random errors, we repeated the aforementioned measurement procedure many times for our primary data sets with and without the external air bearing (five times for figure 2c and thirteen times for figure 8b), each time sweeping the full frequency range of interest and dismounting and remounting both the accelerometers and their mounting plate following each measurement. Well below the shaker resonant frequency, the random errors were typically no greater than ±0.1%.

In addition to measuring the homogeneity of the vertical acceleration, we measure the horizontal (transverse) vibration along the same horizontal line over which we measured the differences in vertical vibration. For these experiments we use the same two accelerometers, now mounting one at the center of the vibrating platform as reference and the other to the side of the accelerometer mounting platform (normal to the upper face of the platform) with its measurement axis passing through the central axis of the shaker. An example of this measurement setup is show in figure 2b. The nominal transverse sensitivity of the accelerometers is ±2.5%, which is consistent with our observed variability in the measured amplitude of horizontal vibration. As a result, measurements of horizontal vibration amplitude are only to be considered significant if they exceed 2.5% of the concurrent vertical vibration amplitude. Similarly, quantitative comparisons between any two measurements of horizontal vibration are not made with any finer resolution.

The horizontal line on the shaker's mounting platform over which we performed all of the measurements in this work was chosen arbitrarily, but the same for all measurements (eg. see figures 2a, 2b, and 12). The results would be very similar had we selected any other line.

We use a National Instruments data acquisition system (NI USB-6343) to acquire data and to generate the driving signal which feeds into the shaker's amplifier. Acquisition and generation was performed at 32 kHz, several orders of magnitude higher than the highest frequency investigated in the present work. The data acquisition system interfaces with a PC using custom Labview software with PI (proportional-integral) feedback control that maintains the vertical vibration amplitude to within $0.002g$ of the specified target value. This accounts for any slow drift in acceleration amplitude that may occur, often a result of the considerable heat generated by the shaker during operation which affects its efficiency [14]. To measure the acceleration amplitude from the accelerometer data, we extract the amplitude of the highest peak in the frequency spectrum, which was always within 0.02% of the input frequency f. Furthermore, to assess the tonal purity of the vibration, we monitored the total harmonic distortion (THD). The THD was compute as the ratio of square root of the sum of the squares of the amplitudes of the harmonics to the amplitude of the fundamental tone. The THD was always less than 0.02 in the present experiments, unless otherwise stated. Note that the THD is a highly non-linear measurement, in particular it increases with increased vibration amplitude. The total root mean square (RMS) amplitude of broad-spectrum noise in our acceleration measurements was less than $0.005g$ for our base test shaker measurements and less than $0.05g$ for our air bearing setup when compressed air was supplied to the linear air bearing. The increase in broad-spectrum noise was due to minor fluctuations in the air supply pressure. However, the increased noise occurred predominantly at high frequencies ($> 10^3$ Hz), resulting in no noticeably increased noise in the amplitude measurements at our test frequencies (20-150 Hz).

The data for this work was collected using a stepwise increase in frequency, with a step size of 2 Hz, over a range of 20 to 150 Hz. After each change in the frequency, we waited for the acceleration amplitude to converge to within $0.02g$ of the target value before collecting data. For measurements of vertical vibration homogeneity, the feedback controller was set to hold the mean acceleration amplitude to a fixed value of $\gamma_V = 4g$. For horizontal vibration measurements, the reference (vertical) accelerometer was set to maintain a fixed amplitude of

$4g$. For all payloads, the static load offsets the equilibrium position of the armature, effectively reducing the maximum achievable peak-to-peak amplitude of the shaker. Thus for heavy payloads, at the lowest frequencies, we necessarily reduced the acceleration amplitude to avoid damaging the shaker. An alternative option would have been to attach an external suspension to the armature or payload, as in [14], which would restore the armature to its unloaded equilibrium position, and the factory specified peak-to-peak range. For the purpose of the present testing, we decided against this option, as this may have introduced further undesirable resonances to the base system, that are no longer directly attributable to the test shaker.

In the next section we proceed by measuring the quality of the vibration of our test shaker in the absence of external modifications.

3. Baseline performance of test shaker

3.1. Test procedure

To perform our baseline performance measurement of the test shaker, we mount a square precision ground aluminum mounting plate (88.9 mm L x 88.9 mm W x 9.5 mm thick) directly to the armature platform. The vertical mounting holes for the accelerometers are spaced 40.4 mm from the center of the platform. To study the influence of the payload weight on the shaker performance, we add an optional number of steel plates (each 152.4 mm L x 152.4 mm W x 6.4 mm thick) beneath the accelerometer mounting plate and atop a second precision aluminum plate (with identical dimensions to the upper plate). Up to four steel plates were added, which corresponded to a total payload of 5.0 kg. The plates (and bolted assembly) were designed to have fundamental frequencies greater than 10^3 Hz, well above our frequency range of interest (20-150 Hz). This ensures that our results are not contaminated by resonances of the payload.

3.2. Results

The first test performed was with a minimal payload (only the mounting plate and accelerometers installed, total payload mass $m = 0.23$ kg), to evaluate the performance of the bare shaker. In figure 2c, we present measurements of differences in the vertical acceleration at two diametrically opposed locations on the mounting plate. For low frequencies ($f \leq 76$ Hz), the forcing is relatively uniform, with differences no greater than 1.0%. However, as the frequency is increased we see that an acceleration bias steadily grows and then rapidly changes orientation, with the difference peaking at $9.2 \pm 1.0\%$ at 124 Hz. From here up to 150 Hz, the magnitude of the difference diminishes.

The shaded region in figure 2c represents the extent of the results of several repeated trials. Following each trial, the mounting plate was rotated 90 degrees and the accelerometers remounted so they continue to measure vertical accelerations along the same line (eg. see figure 2a), relative to the shaker. As can be seen, small discrepancies exists between runs; these are the random errors discussed in section 2. The magnitude of random error was not independent of the test parameters, but was higher near frequencies with significant vibration inhomogeneities, with a maximum of about $\pm 1\%$.

Comparing this data to the corresponding measurement of horizontal vibration presented in figure 2d, we see that the strongest inhomogeneities in the vertical vibration coincide with greatly amplified horizontal vibration. The peak of horizontal vibration occurs at 120 Hz and is $11.2 \pm 2.5\%$ of the vertical vibration amplitude. Since the armature, payload, and support structure have natural frequencies much greater than our test frequency range, we suspect that a resonance of the armature's suspension (internal to the shaker) is excited at these frequencies, which results in the observed non-axial motion.

We remeasure the shaker vertical performance with a heavier payload ($m = 3.9$ kg) as shown in figure 3a and present the results in figure 3b. The performance characteristics have changed dramatically. In particular, appreciable inhomogeneities in the vertical forcing amplitude appear at much lower frequencies than previously. As was the case with a minimal payload, we see that the onset of uneven vertical forcing coincides with strong horizontal vibration, as evidenced in figure 3c. In fact, a single distinct and dominant peak in the horizontal vibration appears for all payloads considered, and is always associated with the onset of inhomogeneities in the vertical vibration. We tested several different payloads, and for each we identified the frequency (f_H) within our range that corresponds to the peak horizontal vibration amplitude, which we refer to as the transverse resonant frequency. The results are plotted in figure 4. A clear monotonic relationship exists: the transverse resonant frequency decreases with the mass of payload, a result one might expect for a simple mechanical resonance. In fact, the data is very well described by a relationship of the form

$$f_H = \frac{1}{2\pi}\sqrt{\frac{k_H}{m}} \tag{1}$$

which is simply the undamped natural frequency of a mass m fixed to a linear spring with stiffness k_H. We find an excellent fit to the data taking $k_H = 0.14$ N/μm, which serves as a rough estimate of the lateral stiffness of the shaker suspension, and allows for the prediction of the first undesirable internal resonance for an arbitrary payload. The excellent agreement provides evidence that the non-axial motion is, as postulated, linked to mechanical resonances internal to the shaker. Moreover, the relative phase of the horizontal and vertical vibration changes most rapidly near the transverse resonant frequency. This effective lateral stiffness is an order of magnitude greater than the axial stiffness of the flexure plates ($k_V = 0.0176$ N/μm, manufacturer specification). Regrettably, there is no measurement of the lateral stiffness provided by the manufacturer with which to compare our estimate.

One seemingly reasonable solution might be to continue to load the shaker (assuming sufficient shaker capacity) to shift the transverse resonant frequency completely below the frequency range of interest. However, it is clear from the results in figure 3b that the performance is not satisfactory even well beyond this principal transverse resonant frequency. Moreover, as the shaker is loaded further, other higher internal resonances are shifted within our frequency range of interest. For our test shaker, in the absence of modifications, the first undesirable internal resonance, as characterized by equation (1), defines a frequency above which the motion is generally irregular.

The results presented in this section should appear troubling to anyone interested in careful forced vibration experiments. Minor changes in frequency or payload can result in potentially drastic changes in vibration performance. One point that cannot be overstressed is that despite the care in which one designs the payload to avoid resonance, significant discrepancies in the vertical vibration amplitude may still appear systemically due to the poor vibration quality provided by the source, the electrodynamic shaker. We also emphasize that the general issues presented here are not peculiar to this particular shaker, or this brand of shakers. Indeed, while the precise characteristics of the internal resonances will differ between models, undesirable performance arising at frequencies well below the armature resonant frequency is common to all flexure-based electrodynamic shakers [5]. The goal of the remainder of this paper is to present a method that will enable us to use the same electrodynamic shaker as a reliable and robust source of uniaxial vibration.

4. Improved design

We present a schematic and image of our improved setup in figure 5. The shaker is fixed to the same leveling platform as described in section 2. The key new feature is the linear air bearing (to be discussed in section 4.1), the carriage of which is mounted to a platform that can be leveled by way of three locking micrometer screws (100 threads per inch), spaced 254 mm from the central axis of the air bearing. These screws are fixed to linear translation stages which allow for adjustment of the lateral alignment of the central axis of the air bearing carriage with the shaker. This assembly is mounted to an optical breadboard with a centered through-hole which in turn rests on four passive air mounts (Barry Controls, SLM-1A). These isolators have a very low natural frequency (~ 3 – 4 Hz) which help to isolate the table and carriage from any floor vibrations. The slider bar of the air bearing is connected to the shaker via a thin drive rod that is stiff in the direction of driving but relatively compliant in all other directions (to be discussed in section 4.2 and shown in figure 6a). On both ends, the rod is inserted into a reamed hole of at least 13 mm depth and set to length before being clamped in place by two diametrically opposed set screws on each end.

Accelerations are measured in a similar manner as before, atop a precision ground aluminum platform (127 mm L x 127 mm W x 12.7 mm thick), now mounted to the top of the air bearing slider bar. The vertical mounting holes for the accelerometers are spaced 54.0 mm from the center of the platform.

4.1. Bearing selection

To constrain the motion of the vibrating platform to a single axis we opted for an air bearing, many advantages of which are described by Slocum [43]. First, they are the smoothest operating of all bearings: the air layer eliminates the influence of any small surface defects. Second, they are unaffected by wear or loss of contact typical of slider or roller bearings. Third, they have no static friction and negligible dynamic friction for our expected operating speeds. Contact bearings have been used in other variations of this experimental setup [19]; however, it was noted that a small amount of position dependent friction resulted in increased harmonic distortion. The gap thickness of an air bearing is generally less than that of hydrostatic bearings, making air bearings preferable for high precision equipment.

We selected a linear air bearing with a square cross section, as this geometry offers impedance to both twisting and lateral motions. To minimize non-axial motion, we would like to maximize the lateral stiffness of the air bearing. The lateral stiffness of a linear air bearing can be estimated as [43]

$$k_{AB} = \frac{0.6(L-a)Wp_s}{h_o}, \tag{2}$$

where L and W are the height and width of the bearing surface, a is the distance from the row of orifices to the outlet of the bearing, p_s is the supply pressure, and h_o is the unloaded gap thickness. From equation 2 it is evident that we would like a large bearing surface, high supply pressure, and small bearing gap. Thus we expect the best results for the largest possible bearing operating at the highest allowable input pressure. We selected a square air bearing composed of anodized aluminum (Nelson Air Corp.) with L = 102 mm, W = 100 mm, a = 20 mm, and h_o = 15 μm. At a supply pressure of p_s = 414 kPa (60 psi), we estimate the bearing stiffness using equation (2) to be k_{AB} = 136 N/μm which is close to the manufacturer specified value of 105 N/μm. We operate the bearing at its maximal supply pressure of p_s = 520 MPa (75 psi), above which we observe instability due to the pneumatic hammer effect. The lateral stiffness of the air bearing exceeds that of the shaker by several orders of magnitude.

4.2. Drive rod selection

The introduction of a thin coupling rod is a common technique used in modal testing of mechanical structures [44]. The thin rods that couple the shaker to the test structure are commonly referred to as “push rods” or “stingers.” Stingers are used in modal testing to allow for efficient transmission of axial forces to the test structure while minimizing lateral constraint forces and moments at the point of attachment. In general, the non-axial stiffnesses of the stinger should be significantly less than those of the test structure in order to avoid serious influences to the measured frequency response function (FRF) [45]. Furthermore, resonances of the stinger should also be avoided or highly damped, as these can readily contaminate the measured FRF [46, 44].

The primary design objectives for a drive rod in our system are similar to those for the stinger used in modal testing. Specifically, we would prefer high axial stiffness (for pure transmission of forces in the axial direction), low lateral and moment stiffnesses (relative to those of the shaker and air bearing), and no stinger resonances. The use of a flexible drive rod in the present system reduces the need for excessive alignment of the air bearing housing with the shaker’s

Symbol	Meaning	Value
E	Young's modulus	205 GPa
ρ	Density	7830 kg m^{-3}
σ_e	Endurance limit	515 MPa
d	Diameter	1.6 mm
L	Length	60 mm
A	$= \pi d^2/4$, Cross-sectional area	2.0 mm^2
I	$= \pi d^4/64$, Area moment of inertia	0.32 mm^4
k	$= 12EI/L^3$, Lateral stiffness	3.7 N/mm
κ	$= 4EI/L$, Moment stiffness	0.077 N-m/deg
M	Mass of payload supported by rod	3.0 kg
m	Mass of entire payload	3.2 kg
f_m	Maximum test frequency	150 Hz
γ_m	Acceleration amplitude	$4g$

Table 1: Symbols, definitions, and design parameters used in the present experiments for a drive rod with uniform circular cross-section.

primary drive axis [1, 10, 12, 16]. As the internal gaps of an air bearing are typically on the order of 10 μm [43], in the absence of a flexible drive rod, micron-resolution in the lateral and angular alignment would be necessary in order to avoid excessive mechanical stresses on the shaker and air bearing assembly. One further advantage of using a flexible drive rod is that it acts as a mechanical fuse between the shaker and payload so that an accidental over forcing of the system will simply lead to the failure of the inexpensive drive rod, rapidly decoupling the shaker from the payload [47].

In what follows, we summarize our principal criteria for the system's drive rod. Note that many of the design principles are naturally transferrable from optimal stinger design [48, 46]. For simplicity and their wide range of availability, we choose to use a solid drive rod with uniform circular cross-section.

We first consider the possibility of axial failure under periodic loading. The amplitude of the cyclical force experience by the rod is simply the product of the mass M of the payload supported by the rod and the peak driving acceleration γ_m. To ensure longevity of the driving rod, we require that the maximum axial stress remains less than the endurance limit σ_e of the selected material. This gives us a minimum rod diameter, d:

$$d > \sqrt{\frac{4M\gamma_m}{\pi\sigma_e}} = d_e. \tag{3}$$

Note that in non-corrosive environments, the value of σ_e is generally independent of loading frequencies below 200 Hz, and independent of size for diameters less than 10 mm [49].

We next consider the possibility of axial or longitudinal resonance. A uniform rod deforms like a linear spring in response to an axial load, with spring constant [50]

$$k_a = \frac{EA}{L}, \tag{4}$$

where E is the rod's Young's modulus, $A = \pi d^2/4$ is its cross-sectional area, and L its length. The drive rod supports a mass M, and is driven from below, as depicted in figure 6b. Provided that the mass, M, of the supported load has a much greater mass than that of the drive rod, this mass-spring system has a natural frequency f_a given by

$$f_a = \frac{1}{2\pi}\sqrt{\frac{\pi E d^2}{4LM}}, \tag{5}$$

where d is the diameter of the drive rod. Beyond the crossover frequency ($f > \sqrt{2} f_a$), the payload will begin to become isolated from the driver, and the transmission of vibration from the shaker to the air bearing slider will be attenuated. It thus becomes increasingly difficult to drive the payload to the desired amplitude [44]. Furthermore, near the axial resonant frequency, we typically measured increased harmonic distortion, possibly due to excitation of the drive rod. To avoid these complications, we require that the axial resonant frequency be greater than the highest frequency in our test range ($f_a > f_m$). We can thus rearrange equation (5) to deduce a restriction on the length of the drive rod:

$$L < \frac{E d^2}{16\pi M f_m^2} = L_a. \tag{6}$$

Given that we aim to drive a relatively heavy load (several kilograms) with a flexible beam, we also need to consider buckling of the drive rod. We design the beam such that it will withstand the maximum axial compressive force expected in our experiments, $|P_m|$. For sinusoidal vibration we can estimate this quantity from Newton's second law,

$$|P_m| = M\left(\gamma_m + g\right) , \tag{7}$$

where γ_m is our maximum driving acceleration. Treating the drive rod as a clamped-clamped beam, we can express the buckling load ($|P_b|$) in terms of the rod parameters [50],

$$|P_b| = \frac{4\pi^2 E I}{L^2} , \tag{8}$$

where $I = \pi d^4/64$ is the area moment of inertia of the rod. To avoid buckling, we require that $|P_b| > |P_m|$. Equivalently, we write a restriction on the length of the drive rod:

$$L < \frac{d^2}{4}\sqrt{\frac{\pi^3 E}{M\left(\gamma_m + g\right)}} = L_b. \tag{9}$$

Finally, we would like to avoid transverse vibrational modes of the drive rod. Near a transverse resonance, any transverse vibrations (introduced by shaker or misalignment of drive rod) could be amplified [51], resulting in large lateral forces or moments applied to the air bearing slider. We thus use an expression for the fundamental transverse frequency of an unloaded uniform beam [50]:

$$f_{l,0} = \frac{\lambda_1^2}{2\pi L^2}\sqrt{\frac{EI}{\rho A}}\ , \tag{10}$$

where ρ is the density of the drive rod material and λ_1^2 is a coefficient that depends on the boundary conditions of the beam, and is approximately 22.4 for a clamped-clamped beam. The natural frequency will be altered by the presence of a constant axial load, as is the case in the present experiments resulting from the static force due to gravity. One can approximate the fundamental transverse frequency of a loaded beam as [52]:

$$f_l = f_{l,0}\sqrt{1 + \frac{P_s}{|P_b|}}\ , \tag{11}$$

where P_s is the constant axial load (negative for compression, positive for tension). Note that for compressive loads, the natural frequency is reduced. Assuming we have adhered to our buckling condition ($|P_b| > |P_m|$), we can thus set a lower bound on the transverse frequency of the loaded beam:

$$f_l > f_{l,0}\sqrt{1 - \frac{g}{\gamma_m + g}} = \beta f_{l,0}\ , \tag{12}$$

where we have taken $P_s = -Mg$. Our correction factor to the unloaded natural frequency is $\beta = \sqrt{1 - \frac{g}{\gamma_m + g}}$ which is less than unity. Thus, finally we require that the maximum driving frequency be less than the loaded transverse frequency ($f_m < f_l$). Rearranging yields a condition on the length of the beam:

$$L < \sqrt{\frac{\beta \lambda_1^2 d}{8\pi f_m}} \left(\frac{E}{\rho}\right)^{\frac{1}{4}} = L_l. \tag{13}$$

If transverse resonances cannot be avoided, surrounding the drive rod in a damping material such as a soft polyurethane foam may improve results by dampening the resonant behavior of the drive rod, a technique demonstrated to be effective for resonant stingers [46].

We have thus arrived at four criteria for drive rod selection: namely the avoidance of fatigue-induced failure (3), buckling (9), axial resonance (6) and transverse resonance (13). For our selected material (W1 tool steel) and the design parameters summarized in Table 1, we can thus isolate our possible design space in the L-d plane, shown as the unshaded region in figure 7a. We immediately see that the maximum length of thin rods is limited by the buckling condition, whereas for thick rods the length is limited by the threat of transverse resonance. Given that the buckling length (L_b) and the length necessary to avoid axial resonance (L_a) both scale with the diameter of the rod squared ($L \sim d^2$), the more restrictive criteria for a particular application will thus be determined by the relative magnitudes of their pre-factors.

Ideally, we would like to select a rod that minimizes both the lateral stiffness (k) and the moment stiffness (κ), described schematically in figures 6c and 6d, respectively. For the present geometry, the lateral stiffness of the rod may be expressed as [48]

$$k = \frac{F}{\delta} = \frac{12EI}{L^3} = \frac{3\pi E d^4}{16L^3}, \tag{14}$$

and the moment stiffness of the rod as

$$\kappa = \frac{\tau}{\theta} = \frac{4EI}{L} = \frac{\pi E d^4}{16L}. \tag{15}$$

We can then replot our design region to show the possible lateral compliances ($1/k$) in figure 7b and moment compliances ($1/\kappa$) in figure 7c, both of which we would ideally like to maximize for our present application. It is clear from these figures that both compliances cannot be maximized simultaneously. However, we can identify a diameter (d_m, here about 2.2 mm) above which both the maximum possible lateral and moment compliances decrease if the rod size is further increased. This maximum diameter occurs here at the crossing point of the buckling and transverse resonance length criteria. This suggests a finite range of possible diameters to select from, $d_e < d < d_m$. In this range it is apparent that the smaller diameters give better moment compliance, while the larger diameters give better lateral compliance. In fact, the maximum product of the compliances, $1/(k\kappa)$, is constant in this region, suggesting the direct trade-off between the two. This can be easily understood, as the product of the compliances will be constant if the length of the rod increases as d^2, which is the same relationship ($L \sim d^2$) as both the buckling and axial resonance restrictions. We compromise by selecting a rod with a diameter near the middle of this region at approximately 50% of its maximum allowable length as a safety factor. Taking such a safety factory will also allow us a small amount of leeway should we later decide to adjust the experimental parameters (e.g. increasing the payload), without having to necessarily change the rod. For our selected rod parameters (d = 1.6 mm, L = 60 mm), we compute a lateral stiffness of 3.7 N/mm, which is several orders of magnitude less than the lateral stiffnesses of both the shaker and of the air bearing. For all of the results in the following section, we will use this drive rod unless otherwise stated.

Finally, we note that had we also considered maximizing the twisting compliance of the rod, the ultimate conclusion would be the same as that for maximizing the moment compliance of the rod (figure 7c). Specifically, we would like the rod be as thin as possible, with the maximum length set by either the buckling or axial resonance condition.

5. Testing of improved design

In figure 8a, we show the accelerometers mounted to the test platform in the configuration for testing the homogeneity of the vertical vibration. These results are presented in figure 8b. The solid line represents the average of thirteen frequency sweeps, while the shaded region indicates the complete range of measurements. As before, following each trial, the mounting plate was rotated 90 degrees and the accelerometers were remounted to assess the influence of random errors. The maximum vertical vibration inhomogeneity has been significantly reduced over the unmodified test shaker (figure 2c) by a factor of approximately 100. There is also an appreciable reduction of random errors over the baseline measurements, with a maximum now of about ±0.3% for the highest frequencies considered, but less than ±0.15% for frequencies below 100 Hz. We also tested the performance after adding an additional 2.8 kg of payload to the mounting plate, the same steel plates used for the baseline testing. The result is given by the dashed line in figure 8. We see that there is no significant difference between the results, indicating that the response is no longer highly sensitive to the payload mass as was the case for the bare shaker. The slight deviations from uniformity appearing in both cases at high frequencies again coincide with an internal resonance of the shaker. We also measured the amplitude of horizontal motion for both the base and heavy payload in figure 8c. In both cases, the maximum horizontal motion is significantly reduced, always measured to be less than the transverse sensitivity of the accelerometers. However, we did measure an increase in the total harmonic distortion at high frequencies for the heavy payload (exceeding 2%). We suspect that this increase was due to the reduction of the drive rod's axial resonant frequency (f_a = 173 Hz) to a value just above our maximum test frequency.

We also explored the effect of decreasing the rod length from L = 60 mm to L = 40 mm while maintaining the same rod diameter, decreasing both the lateral and moment compliances. In figure 9a, we observe an increased amplitude in the deviations from uniform vibration, suggesting that minimizing rod stiffnesses assists in reducing transmission of non-axial motion near a shaker resonance. Again, our measurements of horizontal vibration of the two rods were both less than the transverse sensitivity of the accelerometers, as shown in figure 9b.

Returning to the original $L = 60$ mm rod, we next investigated the influence of an intentional lateral misalignment on the performance. For these experiments we translated the air bearing leveling plate horizontally along the direction of the measurement axis, measuring the distance moved with a digital probe indicator. In figure 10a, we demonstrate that the intentional misalignment introduces an increase in the inhomogeneity of the vertical vibration. The vertical acceleration amplitude is greater on the side of the payload opposite to the direction we move the air bearing carriage. However, the amount by which the inhomogeneity increases is sensitive to the vibration frequency. Once again, our measurements of horizontal vibration of the two rods were always less than the transverse sensitivity of the accelerometers, as shown in figure 10b.

For four frequencies in our test range, we collected additional data to further characterize the effect of misalignment on the vertical vibration homogeneity. The results are presented in figure 11. For each frequency, we find a clear linear relationship between the misalignment distance δ and the difference in vertical vibration amplitudes on opposite sides of the plate, $\Delta\gamma_V$. One might notice that the curves do not all pass precisely through the origin. The shift (most apparent for 150 Hz) is due to internal shaker resonance of which we have seen that a small amount of inhomogeneity persists even for good alignment (recall figure 8b). Overall, these results suggest a straightforward method to calibrate alignment. At a given frequency, several measurements of inhomogeneity can be taken as a function of the lateral translation of either the bearing or shaker, from which the ideal alignment can be easily extrapolated. Additionally, as was also evident in figure 10a, this sensitivity to misalignment increases as the frequency is increased. Despite this shortcoming, one should not lose sight of the fact that the performance is still *significantly* improved over the baseline shaker (figure 2c), even with relatively severe misalignment. We also observed a globally increased sensitivity to misalignment when testing the shorter rod

L = 40 mm, as might be expected. We suspect that there will be a similar performance sensitivity to angular misalignment, although this dependence was not systematically investigated.

Also, by measuring horizontal motion off axis, we found no significant twisting motion in any of the prior test cases, as evidenced in figure 12.

The only performance measurements of a similar system that could be found were reported by Deseigne *et al.* [16]. Their data suggests that above a frequency of about 60 Hz, the maximum difference of vertical vibration amplitude on the platform was never less than approximately 10%. The reason for this relatively large inhomogeneity is not clear. Unfortunately, they do not report the distance from the central axis at which they measure the vertical accelerations, as the measured differences in acceleration due to non-axial, rigid body motion should be linearly dependent on this distance. Furthermore, they use a large polystyrene cone to lift the plate above the air bearing, which places the center of mass of the payload much higher than the point of support, making the payload more susceptible to rocking motions. The selected frequency for their experiments (f = 115 Hz) lies between two apparent yet uninvestigated resonances in the system, easily identified by pronounced localized deviations from homogeneity.

To ensure high-quality vibration, even with the use of an external air bearing and properly designed drive rod, one must also carefully design the payload and the support structure for the air bearing to avoid resonances. For example, a resonance of the air bearing leveling plate will readily contaminate the results, as the carriage itself may no longer be rigidly fixed along a single axis. Throughout our development of the final design, aberrations in performance that were localized in frequency were always underlaid by some mechanical resonance in the system. Once identified, the component could be redesigned and the performance substantially improved. In general, we noticed that the improved system discussed herein was remarkably robust at low frequencies; however, more careful alignment and component design became necessary at higher frequencies.

The potential influence of drive rod resonances can easily be checked by varying the rod length and assessing whether the spurious resonant frequencies shift. If not, it is likely that the aberrations are caused by the resonance of some other component in the system.

6. Conclusions

We have demonstrated the efficacy of introducing a linear air bearing to rectify the non-axial motions typical of flexure-based electrodynamic shakers. We tested a standard shaker and observed a distinct mechanical resonance of the armature's suspension leading to non-axial motion of the payload. We have also demonstrated that the performance of the unmodified shaker is sensitive to the details of the payload, including its mass. This resonance introduces large inhomogeneities in the vertical vibration amplitude as well as significant transverse vibrations of the armature. The frequencies considered are well below the resonant frequency of either the armature itself or the payload, and are typical of experimental investigations of vibrated granular materials, Faraday waves, and walking droplets.

We have presented the details of an improved design that incorporates an external air bearing to eliminate torsional motion and more effectively constrain the vibration to a single axis. We have provided general criteria for selection of a drive rod that couples the shaker to the air bearing slider. We have also presented our test results, which demonstrated a significant improvement of the vibration quality of the payload for our entire frequency range of interest (20-150 Hz). In particular, our design reduced the maximum inhomogeneity of the vertical vibration amplitude from approximately 10% to 0.1%. The details of our results have allowed us to arrive at several important conclusions concerning our new design. First, the performance is relatively insensitive to the mass of the payload, in stark contrast to the baseline shaker results. Second, minimizing the non-axial stiffnesses of the drive rod reduces the transmission of non-axial motions to the drive platform. Finally, we reported a linear dependence of the inhomogeneity of vertical vibration on the lateral alignment of the air bearing with the shaker. In all tests performed with the improved setup, the horizontal vibration and any potential twisting motions of the platform were too small to be detected by the accelerometers.

While the mild sensitivity to alignment might be seen as a shortcoming, it could also prove useful for certain investigations. In particular, intentional misalignment seems to be a controllable way to introduce imhomogeneous vibration into the system. One might thus investigate the influence of mildly inhomogeneous vibration on pattern formation in Faraday waves or on the trajectories of walking droplets.

Most recently, we utilized this vibration system in our study of droplets walking on a vibrated rotating bath [37]. We demonstrated that just below the Faraday threshold, the dynamical and statistical behavior of the droplets is extremely sensitive to the driving amplitude. Reliable results thus required the highly uniform driving and precise control of the forcing amplitude made possible by our improved vibration system. We are presently revisiting several key experiments in the field of hydrodynamic quantum analogues, in particular the diffraction of walking droplets by single- and double-slit geometries [34] and droplets confined to cavities [40], with previously unattainable control of the forcing amplitude. We hope that these studies will yield further insight into the quantum-like behavior of walking droplets [33].

The authors gratefully acknowledge the financial support of the NSF through grants CBET-0966452 and CMMI-1333242; D.M.H. was supported through the Graduate Research Fellowship Program. The authors thank P. Reis and D. Goldman for valuable discussions.

References

[1] D.I. Goldman, Pattern formation and fluidization of vibrated granular layers, and grain dynamics and jamming in a water fluidized bed. Ph.D. thesis, University of Texas at Austin, Austin, TX (2002)

[2] G.F. Lang, Sound and Vibration **31**(4), 14 (1997)

[3] G.F. Lang, D. Snyder, Sound and Vibration **35**(10), 24 (2001)

[4] G.P. Ripper, R.S. Dias, G.A. Garcia, Measurement **42**(9), 1363 (2009)

[5] R.W. Bono, E.J. Seller, Cal Lab-International Journal of Metrology **18**(1), 31 (2011)

[6] ISO, Methods for the calibration of vibration and shock transducers – Part 21: Vibration calibration by comparison to a reference transducer. ISO 16063-21:2003, International Organization for Standardization, Geneva, Switzerland (2003)

[7] T. Dimoff, B.F. Payne, Journal of Research of the National Bureau of Standards **67**(4), 327 (1963)

[8] J. Dosch, in *Proceedings of the 24th International Modal Analysis Conference* (2006)

[9] J.R. de Bruyn, B.C. Lewis, M.D. Shattuck, H.L. Swinney, Phys. Rev. E **63**, 041305 (2001)

[10] P.M. Reis, R.A. Ingale, M.D. Shattuck, Phys. Rev. E **75**, 051311 (2007)

[11] Z. Daya, E. Ben-Naim, R. Ecke, The European Physical Journal E **21**(1), 1 (2006)

[12] J.A. Dijksman, M. van Hecke, Europhys. Lett. **88**(4), 44001 (2009)

[13] J.A. Dijksman, G.H. Wortel, L.T. van Dellen, O. Dauchot, M. van Hecke, Phys. Rev. Lett. **107**(10), 108303 (2011)

[14] G.H. Wortel, J.A. Dijksman, M. van Hecke, Phys. Rev. E **89**(1), 012202 (2014)

[15] J. Deseigne, O. Dauchot, H. Chaté, Phys. Rev. Lett. **105**(9), 098001 (2010)

[16] J. Deseigne, S. Léonard, O. Dauchot, H. Chaté, Soft Matter **8**(20), 5629 (2012)

[17] N. Gravish, S.V. Franklin, D.L. Hu, D.I. Goldman, Phys. Rev. Lett. **108**(20), 208001 (2012)

[18] A. Boudaoud, E. Hamm, F. Melo, Phys. Rev. Lett. **99**(25), 254301 (2007)

[19] P.B. Umbanhowar, Wave patters in vibrated granular layers. Ph.D. thesis, University of Texas at Austin, Austin, TX (1996)

[20] H.K. Pak, E. Van Doorn, R.P. Behringer, Phys. Rev. Lett. **74**, 4643 (1995)

[21] I.S. Aranson, D. Volfson, L.S. Tsimring, Phys. Rev. E **75**(5), 051301 (2007)

[22] V. Narayan, S. Ramaswamy, N. Menon, Science **317**(5834), 105 (2007)

[23] C.L. Goodridge, W.T. Shi, D.P. Lathrop, Phys. Rev. Lett. **76**(11), 1824 (1996)

[24] W.T. Shi, C.L. Goodridge, D.P. Lathrop, Phys. Rev. E **56**(4), 4157 (1997)

[25] C. Huepe, Y. Ding, P. Umbanhowar, M. Silber, Phys. Rev. E **73**(1), 016310 (2006)

[26] Y. Ding, P. Umbanhowar, Phys. Rev. E **73**(4), 046305 (2006)

[27] M. Faraday, Philos. Trans. R. Soc. London **121**, 319 (1831)

[28] J. Miles, D. Henderson, Ann. Rev. of Fluid Mech. **22**, 143 (1990)

[29] T. Besson, W.S. Edwards, L.S. Tuckerman, Phys. Rev. E **54**(1), 507 (1996)

[30] J. Bechhoefer, V. Ego, S. Manneville, B. Johnson, J. Fluid Mech. **288**, 325 (1995)

[31] S. Protière, A. Boudaoud, Y. Couder, J. Fluid Mech. **554**, 85 (2006)

[32] J. Moláček, J.W.M. Bush, J. Fluid Mech. **727**, 612 (2013)

[33] J.W.M. Bush, Ann. Rev. of Fluid Mech. **47** (2014, *to appear*)

[34] Y. Couder, E. Fort, Phys. Rev. Lett. **97**, 154101 (2006)

[35] A. Eddi, E. Fort, F. Moisy, Y. Couder, Phys. Rev. Lett. **102**, 240401 (2009)

[36] E. Fort, A. Eddi, A. Boudaoud, J. Moukhtar, Y. Couder, Proc. Nat. Acad. Sci. **107**(41), 17515 (2010)

[37] D.M. Harris, J.W.M. Bush, J. Fluid Mech. **739**, 444 (2014)

[38] A.U. Oza, D.M. Harris, R.R. Rosales, J.W.M. Bush, J. Fluid Mech. **744**, 404 (2014)

[39] S. Perrard, M. Labousse, M. Miskin, E. Fort, Y. Couder, Nature Comm. **5** (2014)

[40] D.M. Harris, J. Moukhtar, E. Fort, Y. Couder, J.W.M. Bush, Phys. Rev. E **88**, 011001 (2013)

[41] S. Protière, Y. Couder, E. Fort, A. Boudaoud, Journal of Physics: Condensed Matter **17**(45), S3529 (2005)

[42] O. Wind-Willassen, J. Moláček, D.M. Harris, J.W.M. Bush, Phys. Fluids **25**, 082002 (2013)

[43] A.H. Slocum, *Precision Machine Design* (Prentice-Hall, 1992)

[44] D.J. Ewins, *Modal testing: theory, practice and application* (Research Studies Press, Baldock, Hertforshire, England, 2000)

[45] D. Cloutier, P. Avitabile, R. Bono, M. Peres, in *Proceedings of the 27th International Modal Analysis Conference* (2009), pp. 9–12

[46] I. Anderson, in *Proceedings of the 8th International Modal Analysis Conference* (1990), pp. 673–678

[47] M.A. Peres, R.W. Bono, D.L. Brown, in *Proceedings of ISMA 2010* (2010), pp. 2539–2551

[48] G. Hieber, in *Proceedings of the 6th International Modal Analysis Conference* (1988), pp. 1371–1379

[49] R.I. Stephens, H.O. Fuchs, *Metal fatigue in engineering* (J. Wiley, New York)

[50] R.D. Blevins, *Formulas for Natural Frequency and Mode Shape* (Van Nostrand Reinhold, 1979)

[51] R. Bishop, D. Johnson, *The mechanics of vibration* (1960)

[52] A. Bokaian, J. Sound and Vibration **126**(1), 49 (1988)

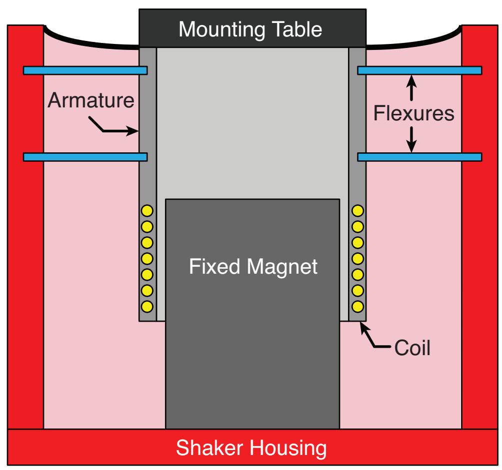

Figure 1: Simplified schematic of cross-section of a typical electrodynamic flexure-suspension shaker.

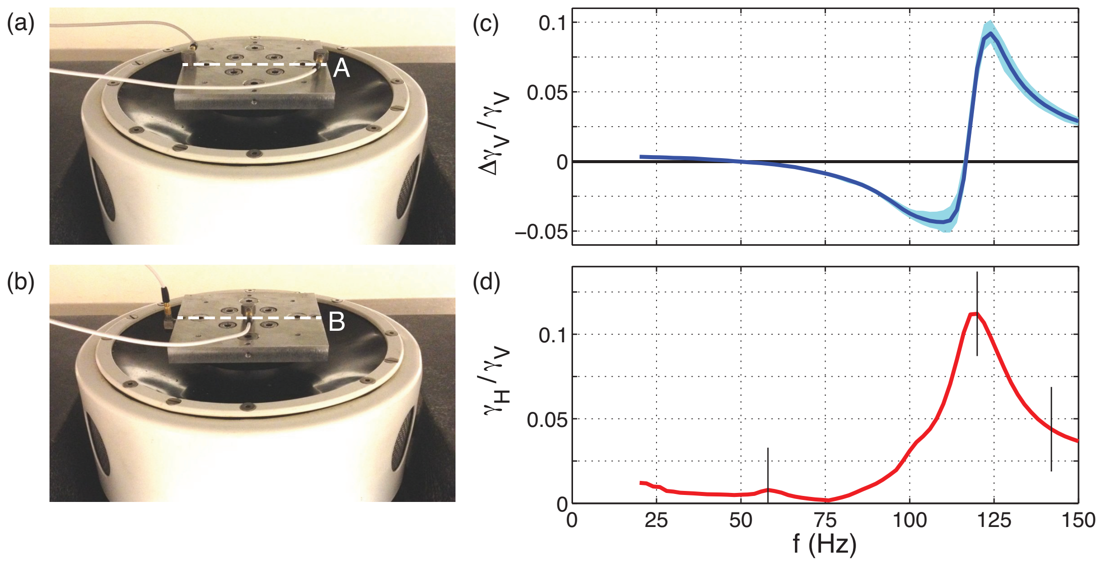

Figure 2: Performance of test shaker with payload of $m = 0.23$ kg, as shown in (a) and (b). The dashed lines labeled A and B indicate the horizontal line over which all measurements were taken. (c) Normalized difference in vertical acceleration amplitude measured in two diametrically opposed locations on accelerometer mounting plate as shown in (a). The solid line is the mean of five frequency sweeps, while the the shaded region indicates the complete range of measurements. (d) Acceleration amplitude of horizontal vibration, measured as shown in (b). Characteristic error bars corresponding to the transverse sensitivities are shown.

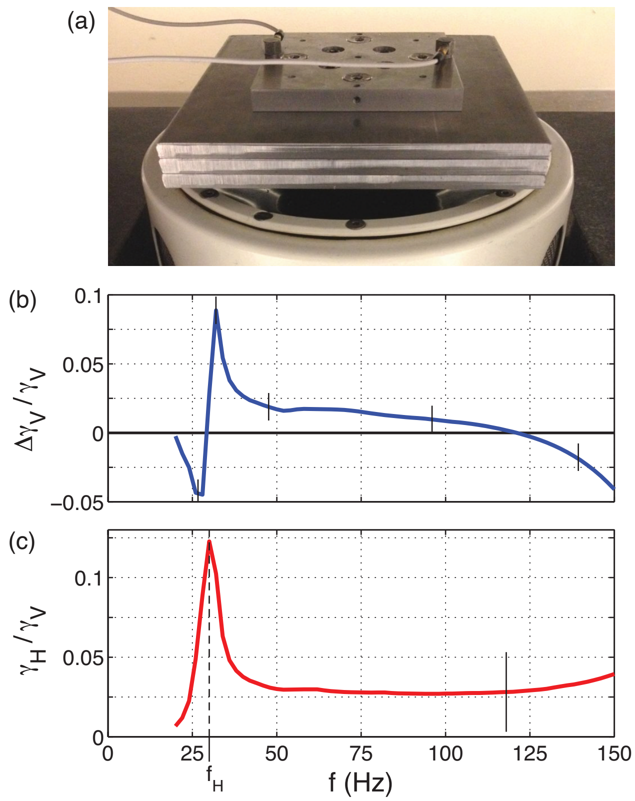

Figure 3: Performance of test shaker with payload of m = 3.9 kg, as shown in (a). (b) Normalized difference in vertical acceleration amplitude measured in two diametrically opposed locations on mounting plate. Characteristic error bars corresponding to estimated random errors are shown. (c) Acceleration amplitude of horizontal vibration. The peak of lateral acceleration amplitude in the frequency range of interest is identified as f_H, here at 30 Hz.

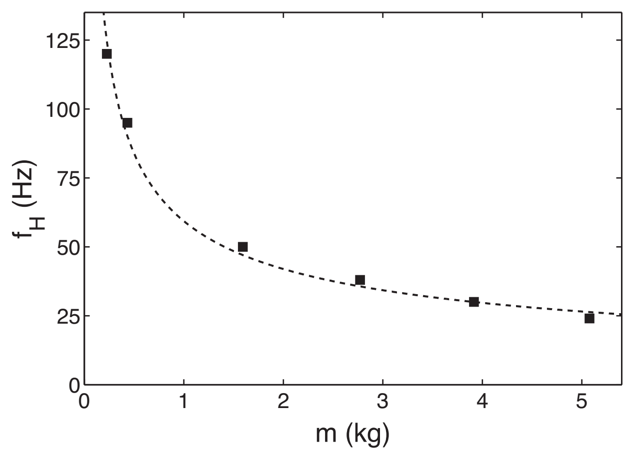

Figure 4: The dependence of f_H on payload mass m. The experimental data (■) is well described by a curve (dashed line) of the form given by equation (1) with $k_H = 0.14$ N/μm.

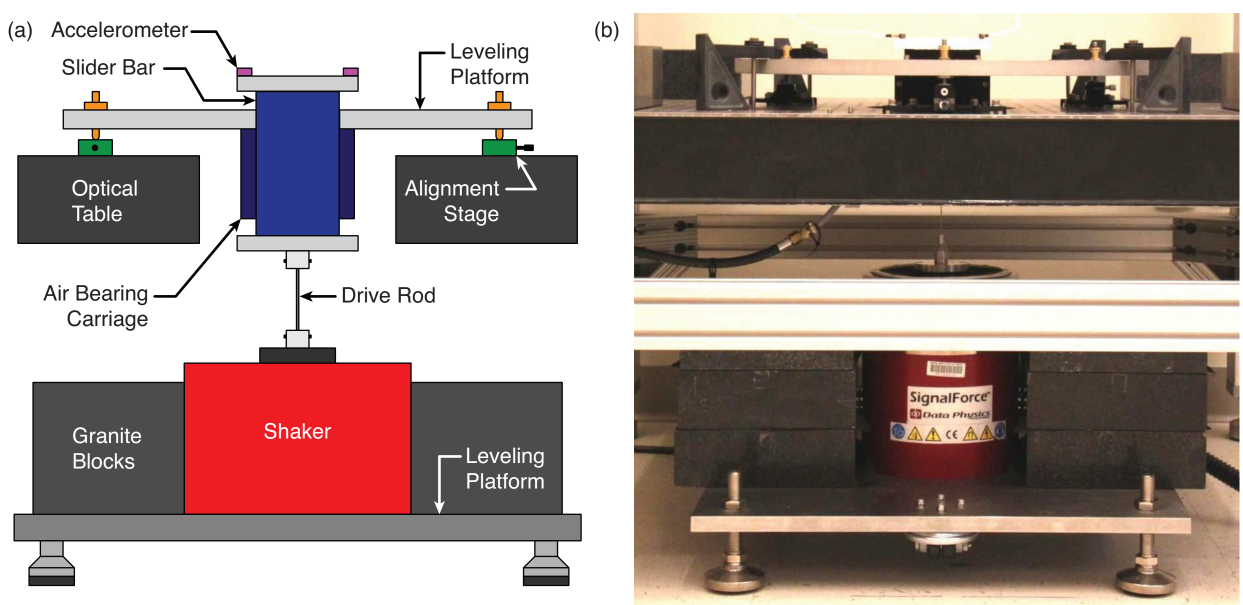

Figure 5: (a) Schematic and (b) image of the improved setup with external air bearing.

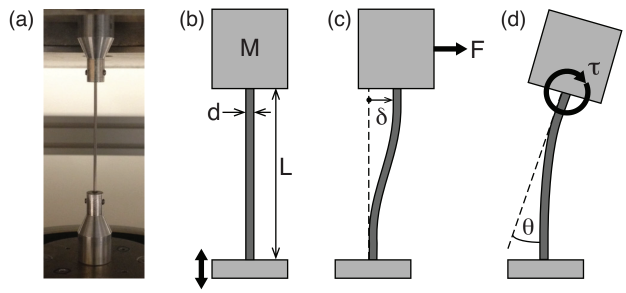

Figure 6: (a) Close-up image and (b) schematic of drive rod. Diagrams defining the (c) lateral stiffness, $k = F/\delta$, and (d) moment stiffness, $\kappa = \tau/\theta$, of the drive rod.

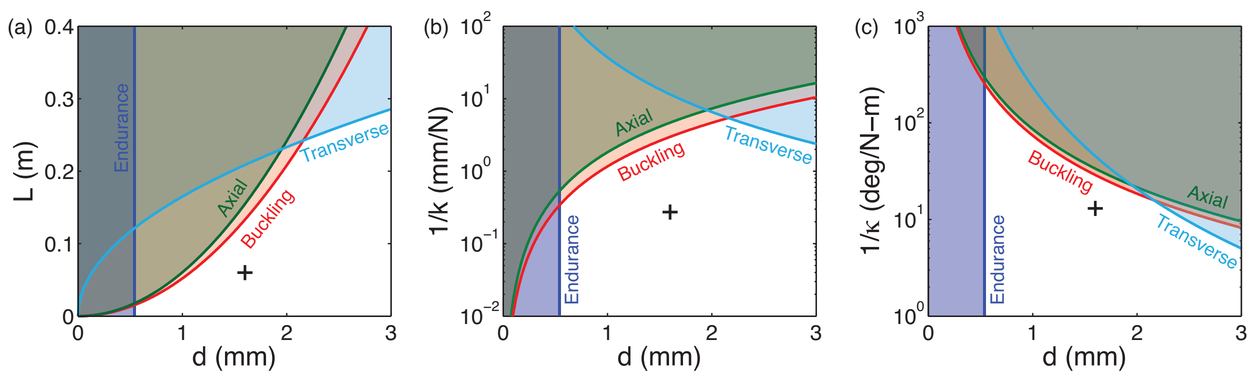

Figure 7: (a) Design region for drive rod, (b) lateral compliances of design region, and (c) moment compliances of design region. The curves represent bounds based on the avoidance of endurance-induced failure (3), axial resonance (6), buckling (9), and transverse resonance (13) as labeled, using the quantities from table 1. The shaded regions are forbidden or inaccessible due to at least one of these criteria. The marker identifies the location of the selected drive rod for the present application.

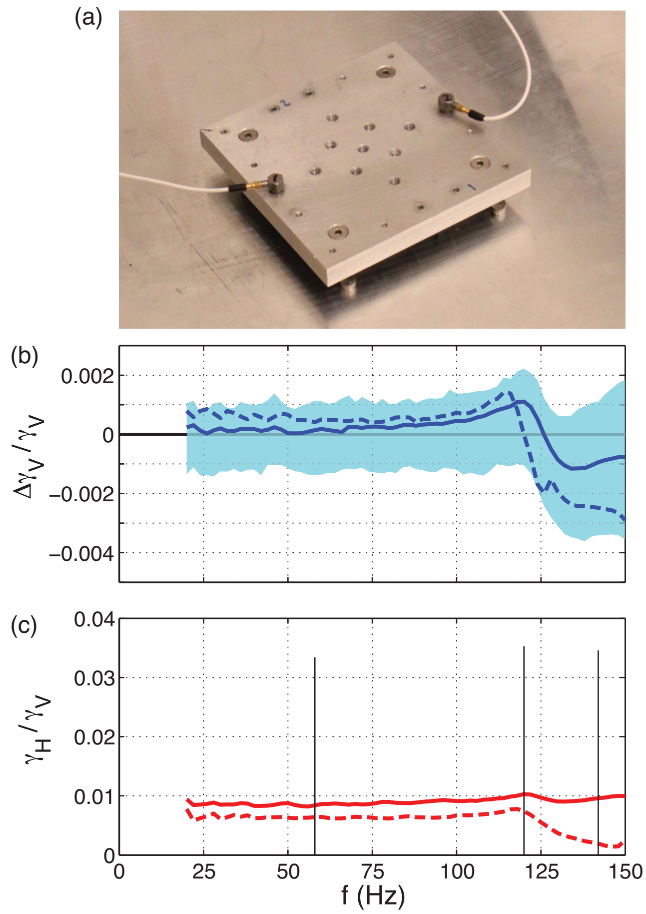

Figure 8: (b) Normalized difference in vertical acceleration amplitude measured in two diametrically opposed locations atop the air bearing slider as shown in (a). The solid line is the mean of thirteen frequency sweeps with a total shaker payload of m = 3.2 kg, while the shaded region indicates the complete range of measurements. The dashed line represents a measurement with an additional 2.8 kg mounted atop the slider bar. (c) Acceleration amplitude of horizontal vibration, with a base payload (m = 3.2 kg, solid line) and a heavy payload (m = 6.0 kg, dashed line).

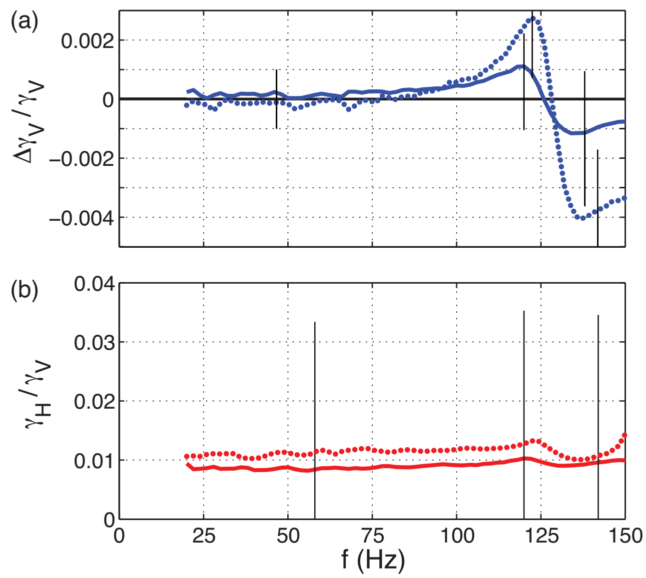

Figure 9: (a) Normalized difference in vertical acceleration amplitude measured in two diametrically opposed locations atop the air bearing slider with base payload (m = 3.2 kg). The solid line is the result for the drive rod of length L = 60 mm. The dotted line is the result for the drive rod of length L = 40 mm, with the same diameter. Characteristic error bars corresponding to estimated random errors are shown. (b) Acceleration amplitude of the corresponding horizontal vibrations.

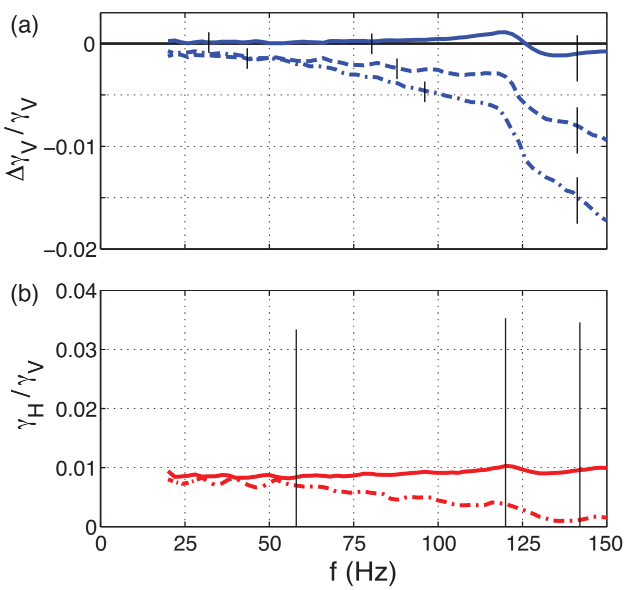

Figure 10: (a) Normalized difference in vertical acceleration amplitude and (b) acceleration amplitude of horizontal vibration atop the air bearing slider with different amounts of lateral misalignment along test axis between air bearing housing and shaker (solid line, δ = 0.0 mm; dashed line, δ = 0.4 mm; dash-dot line, δ = 0.8 mm).

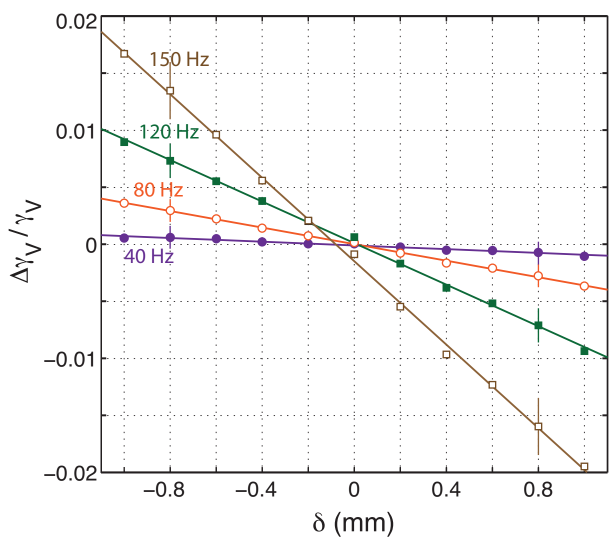

Figure 11: Normalized difference in vertical acceleration as a function of lateral misalignment (δ) along the test axis between air bearing housing and shaker for four different test frequencies. The lines are linear fits to the respective data sets. Characteristic error bars corresponding to estimated random errors are shown.

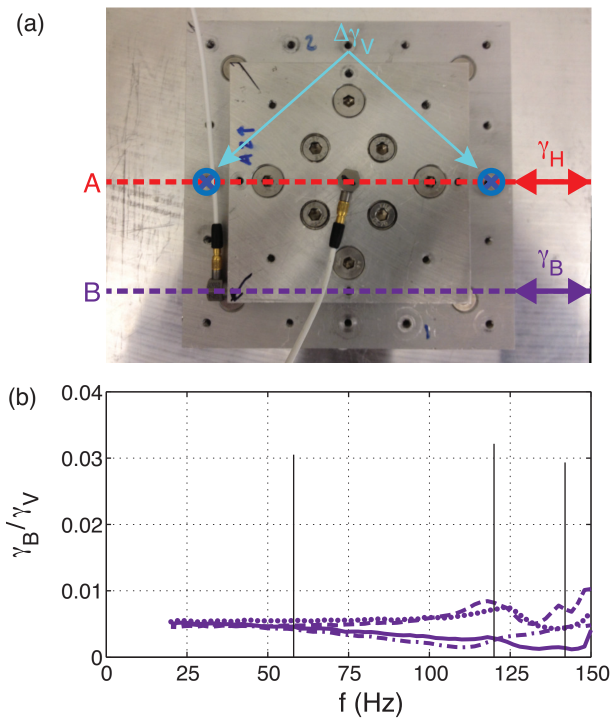

Figure 12: (a) Image of the accelerometer mounting plate for the air bearing setup. To assess the possibility of twisting motions, we also measure the horizontal vibration amplitude along line B (γ_B), which is 40.4 mm off of the central axis of the shaker. The measurements of the horizontal vibration amplitude, γ_H, were taken along line A. (b) Acceleration amplitude of horizontal vibration (γ_B). The solid line is the result with a drive rod of length L = 60 mm, total payload m = 3.2 kg, and lateral misalignment δ = 0.0 mm; the dashed line is with L = 60 mm, m = 6.0 kg, δ = 0.0 mm; the dotted line is with L = 40 mm, m = 3.2 kg, δ = 0.0 mm; and the dash-dot line is with L = 60 mm, m = 3.2 kg, δ = 0.8 mm.